

Coherent structures in reaction-diffusion models for precipitation¹

Ryan Goh
Department of Mathematics
Michigan State University
East Lansing, MI 48824

Samantha Mesuro
Harvey Mudd College
301 Platt Boulevard
Claremont, CA 91711

Arnd Scheel
University of Minnesota
School of Mathematics
206 Church St. S.E.
Minneapolis, MN 55455

Abstract

We study a class of models for precipitation from a dynamical systems point of view. The class of models incorporates Cahn-Hilliard-type models for spinodal decomposition and supersaturation theories as natural limiting cases. We analyze existence and stability of coherent structures, and relate our findings to simulations of Liesegang pattern formation.

1 Introduction

Among a plethora of models that have been proposed for the study of recurrent precipitation, reaction-diffusion models stand out as an easily tractable class, from both an analytic and from a numerical point of view. Our goal here is to put some of these models into a broader context and point out similarities and differences. Our view point will be a dynamical systems one, where we focus on existence and stability of coherent structure. To be precise, consider a reaction-diffusion system

$$\begin{aligned}c_t &= c_{xx} - f(c, e) + h(t, x) \\ e_t &= de_{xx} + f(c, e),\end{aligned}\tag{1.1}$$

where c, e are concentrations of a chemical species in solution, c , or when precipitated, e . The diffusion constant of c is normalized to 1 and the diffusion constant d of e will be assumed to be small, $d < 1$. The term $h(t, x)$ is a source term which models the output of a chemical reaction that generates the species c ; an example is $h = ab$, where a and b are the concentrations of species A and B in a simple bimolecular reaction $A + B \rightarrow C$. The nonlinear conversion rate f is assumed to exhibit some type of threshold behavior, which we comment on later. We study a one-dimensional setup $x \in [0, L]$, and assume that the domain is large, so that $x \in \mathbb{R}$ often provides a good approximation. The basic strategy is to study stationary states and traveling waves in a situation where f is smooth and d is nonzero. We view the important cases of non-smooth kinetics f and zero-diffusion $d = 0$ as limiting cases.

2 Threshold kinetics

Throughout, we assume that kinetics are of *threshold type*. More precisely, we assume that there is a smooth curve of equilibria $f(c, e) = 0$ for $c + g(e) = 0$, and $g' < 0$ for $e \in (-\infty, e_-) \cup$

¹The authors gratefully acknowledges support by the National Science Foundation under grant NSF-DMS-0806614.

$(e_+, +\infty)$, and $g' > 0$ for $e \in (e_-, e_+)$. In other words, in equilibrium the concentration of e is increasing when the concentration of c is increasing for large or small values of e . For intermediate concentrations of c , however, the equilibrium concentration of the precipitate e may decrease although the concentration in solution c increases. The simplest example of such nonlinearities is a cubic nonlinearity

$$f(c, e) = \gamma(g(e) + c), \quad g(e) = \kappa e(1 - e)(e - a), \quad \kappa, \gamma > 0, \quad (2.1)$$

so that $e_{\pm} = \frac{1}{2}(1 + a \pm \sqrt{1 - a + a^2})$. Shifting $e = e - e_0$, $c = c - c_0$, appropriately, one can in fact guarantee that positivity of c, e is preserved by the dynamics.

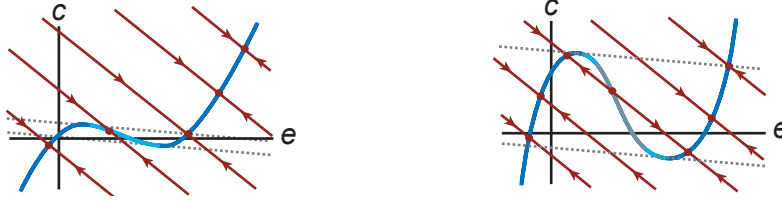


Figure 2.1: *Phase portraits for cubic spinodal (left) and bistable (right) kinetics. The dashed line marks the boundaries of stability for the PDE; see Section 5.*

Such systems are in fact equivalent to a phase-field equation [5], with “temperature” $\theta = c + de$ and an “order parameter” e ,

$$\begin{aligned} \theta_t + (1 - d)e_t &= \theta_{xx} + h(t, x) \\ e_t &= de_{xx} + f(\theta - de, e). \end{aligned}$$

When $f(c, e) = \gamma(g(e) + c)$ and $h \equiv 0$, the system possesses a free energy

$$W(e, c) = \int \frac{1}{2} de_x^2 + \gamma \left(G(e) + \frac{1}{2} \left(c^2 + \frac{d}{1-d} (c + e)^2 \right) \right), \quad (2.2)$$

with $G' = -g$. The system is in fact a gradient flow with this energy, with metric factor $\mathcal{M} = \mathcal{M}^* \geq 0$, so that

$$\begin{pmatrix} c_t \\ e_t \end{pmatrix} = -\mathcal{M} \nabla_{L^2} W, \quad \mathcal{M} = \begin{pmatrix} \text{id} - \frac{1-d}{\gamma} \partial_{xx} & -\text{id} \\ -\text{id} & \text{id} \end{pmatrix}. \quad (2.3)$$

Of course, the structure of a gradient flow puts narrow constraints on which kinds of dynamics are possible. One can, for instance, readily exclude various forms of oscillations. On the other hand, systems with a more general form of f may still possess gradient or gradient-like structures, even if we do not know of an explicit energy. In all cases, the dynamics of spatially homogeneous profiles are gradient-like, since they are essentially one-dimensional due to the constraint $\frac{d}{dt}(c(t) + e(t)) \equiv 0$; see Figure 2.1.

3 Limiting cases I: Cahn-Hilliard and Allen-Cahn

For κ small in (2.1), that is, for weak dependence of the c -equilibrium concentration on the e -concentration, one can scale x, t, θ , and d so that the new system is

$$\begin{aligned}\varepsilon\theta_t + e_t &= \theta_{xx} + \tilde{h}(t, x) \\ \varepsilon e_t &= de_{xx} + \tilde{g}(e) + \theta.\end{aligned}$$

In the limit $\varepsilon = 0$, this system is equivalent to the Cahn-Hilliard equation

$$e_t = -(de_{xx} + \tilde{g}(e))_{xx} + \tilde{h}(t, x).$$

We refer to [7] for convergence results in the singular limit, and to [1],[2],[6] for the role of Cahn-Hilliard phase separation models in precipitation phenomena.

In the opposite limit, κ large, the dynamics limit (regularly) after scaling on

$$\begin{aligned}c_t &= c_{xx} - g(e) \\ e_t &= de_{xx} + g(e).\end{aligned}$$

One can then solve the e -equation independently of the c -equation. For threshold kinetics g , the e -dynamics are given by Allen-Cahn dynamics, with well understood front and layer dynamics. We refer to [4] for some perturbation results from this (regular) limit.

4 Limiting cases II: Supersaturation theory

Keller and Rubinow [13] proposed a supersaturation model with piecewise linear kinetics for f ,

$$f_{\text{sat}}(c, e) = \begin{cases} 0 & \text{for } c < c_*(e), \\ c - c_s & \text{for } c \geq c_*(e) \end{cases}, \quad \text{where } c_*(e) = \begin{cases} c_s > 0 & \text{for } e > 0, \\ c_{\text{ss}} > c_s & \text{for } e = 0 \end{cases}. \quad (4.1)$$

In this specific, piecewise linear form of the kinetics, one can actually prove recurrent spiking with suitable input function h ; see [11, 12, 13].

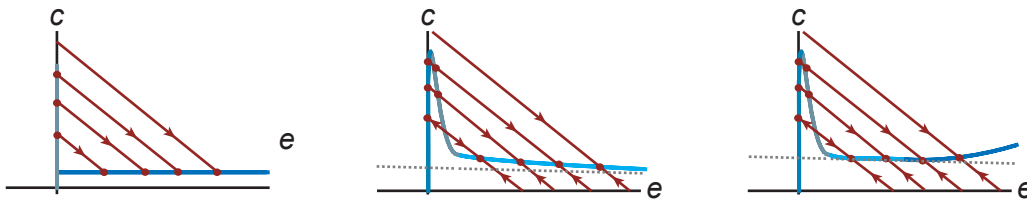


Figure 4.1: *Phase portraits for the Keller-Rubinow super-saturation kinetics (left), and for the smoothed versions g_1, g_2 (middle and right). Tangencies with the dashed curve $c+de = \text{const}$ mark stable-spinodal transitions; see Section 5.*

Non-smooth kinetics together with vanishing diffusion make the concept of a solution somewhat subtle [11]. As we shall see, the Keller-Rubinow model is in many ways structurally

unstable: approximating it by smooth kinetics with small diffusion can yield qualitatively different results depending on the approximation. The kinetics (4.1) can be approximated by smooth functions $f_j(c, e) = g_j(e) + c$, with $g_j = g_j^\delta$, so that nullclines converge as $\delta \rightarrow 0$, for instance using

$$\begin{aligned} g_1(e) &= -\beta\left(\frac{e}{\delta} - \alpha\right)e^{-\frac{e}{\delta}} - 1, \\ g_2(e) &= -\beta\left(\frac{e}{\delta} - \alpha\right)e^{-\frac{e}{\delta}} - 1 + \delta e, \end{aligned} \quad (4.2)$$

with appropriate constants $\alpha, \beta > 0$. While both functions g_j give nullclines that converge to the Keller-Rubinow nullclines, there are subtle differences. Only g_2 gives threshold kinetics as defined above: $g_1'(e) > 0$ for all e large, $g_2'(e) < 0$ for e large; see Figure 4.1 for ODE phase portraits and nullclines, and, for instance, Figure 12.1 for an effect on patterns.

5 Equilibria and instabilities

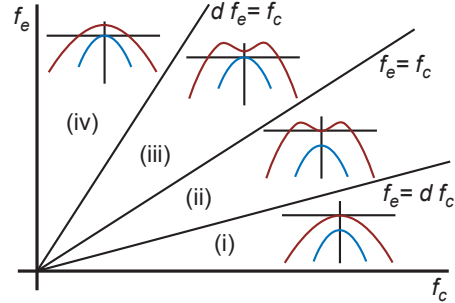
We briefly investigate linearized stability of equilibria $f(c_*, e_*) = 0$ for $x \in \mathbb{R}$. Stability with Neumann or periodic boundary conditions is easily inferred. Eigenvalues λ of the linearized system are given by

$$\lambda_{\pm} = \frac{1}{2}(\text{tr} \pm \sqrt{\text{tr}^2 - 4 \det}), \quad \text{tr} = f_e - f_c - (1 + d)k^2, \quad \det = (df_c - f_e)k^2 + dk^4, \quad k \in \mathbb{R} \quad (5.1)$$

and $f_j := \partial_j f(c_*, e_*)$. We focus on the case $f_c > 0, d < 1$.

One finds four qualitatively different regions,

- (i) *stable*: when $f_c > df_c > f_e$.
- (ii) *spinodal*: when $f_c > f_e > df_c$.
- (iii) *homogeneous unstable I*: when $f_e > f_c > df_e$.
- (iv) *homogeneous unstable II*: when $f_e > df_e > f_c$.



Our assumption on threshold kinetics guarantees that equilibria are stable for $e \notin (e_-, e_+)$. We will say that the kinetics are of bistable type if there exists a region where equilibria are homogeneous unstable. In the case of cubic $g(e) = \kappa e(1 - e)(e - a)$, bistability occurs for $\kappa > 4$. Note that the smoothed versions of super-saturation theories always exhibit bistability, whereas in the regime where dynamics are close to Cahn-Hilliard dynamics, the kinetics only possess spinodal regions.

6 Stationary patterns

Due to the conservation law, time-independent patterns satisfy a scalar equation

$$de_{xx} + f(\mu - de, e) = 0, \quad c + de = \mu. \quad (6.1)$$

Bounded, spatially non-constant solutions to this equation are either periodic, homoclinic (spikes), or heteroclinic (layers). Rescaling $y = x/\sqrt{d}$, one finds that, in the limit $d = 0$,

patterns converge to solutions of $e_{yy} + f(\mu, e) = 0$. Layers exist only at Maxwell points, when $V(e; \mu) = \int f(\mu - de, e)de$ possesses critical points $V'(e_{\pm}; \mu) = 0$ at equal levels $V(e_+; \mu) = V(e_-; \mu)$. Cubic models can readily be seen to possess unique Maxwell points. The supersaturation models, however, turn out to lie at the boundary of the set of functions f that allow for Maxwell points. One can verify that the somewhat non-standard smoothed kinetics h_2 in (4.2) possess layers, while layers of the simpler kinetics h_1 diverge as $d \rightarrow 0$. We also note that mass is not conserved across layers, that is $e + c =: m(x)$ possesses different limits as $x \rightarrow \pm\infty$. Indeed, since $c + de$ is constant along a stationary pattern, $e + c$ cannot be constant when $d \neq 1$. In other words, layers separate regions in physical space with different total concentrations $c + e$.

The following general result shows that only layers are stable when considered as patterns on large domains for (1.1) (and actually a much larger class of systems).

Proposition 6.1 [14, 15] *Spikes and periodic solutions are linearly and nonlinearly unstable when considered as solutions on the whole real line, or on a sufficiently large domain with periodic or Neumann boundary conditions. Layers are stable when the system possesses a variational structure.*

The situation is slightly more subtle when periodic (or Neumann) boundary conditions with period L are imposed for a periodic pattern of period L . Define the mass m as the average total concentration $m = L^{-1} \int_0^L (e + c)$, and recall the definition of $\mu = c + de$ as a pointwise conserved quantity. One can typically (always for cubic nonlinearities), find a family of periodic patterns with fixed period L as a function of μ , and thereby define $m = m(\mu)$.

Proposition 6.2 [15] *Suppose that the system possesses a variational structure. Then periodic solutions are stable when considered with periodic boundary conditions corresponding to their minimal period, if $m'(\mu) < 0$. Periodic patterns with $m'(\mu) > 0$ are unstable.*

We note that for masses without stable equilibria, there necessarily exists a stable periodic pattern that can be constructed as a minimizer of the energy. We do not know if stable periodic patterns exist in bistable regimes. The instability statements are true for systems without a variational structure. Stability holds whenever one can exclude Hopf bifurcations, which appears to be a good modeling assumption for precipitation phenomena.

We briefly comment on traveling waves $(c, e)(x - st)$, $s > 0$. In (θ, e) -variables, traveling waves satisfy the ODE

$$\begin{aligned} \theta_{\xi} &= -s(\theta + (1 - d)e - m_{\infty}) \\ e_{\xi} &= w \\ w_{\xi} &= -d^{-1}(sw + f(\theta - de, e)). \end{aligned} \tag{6.2}$$

Here m_{∞} , an integration constant, equals the mass $e_{\infty} + c_{\infty}$, which is conserved across the traveling wave: $\lim_{\xi \rightarrow \pm\infty} (c + e)(\xi) = m_{\infty}$. Existence of traveling waves has been studied in several limiting scenarios, such as $d \ll 1$ and $\kappa \gg 1$; see for instance [3, 4, 9, 8]. Typically, one can show existence of traveling waves connecting stable equilibria. For $d \ll 1$ comprehensive

existence and uniqueness results are available, but only little appears to be known about stability.

7 Instability and linear wavenumber selection

We imagine a situation where parameters (or concentrations) are changed adiabatically so that the system is quenched into an unstable, spatially homogeneous state. One can then ask for the wavelength of the pattern that is created by a small perturbation of the pattern. There are (at least) two fundamental mechanisms for wavenumber selection in such a situation.

First, a spatially random perturbation would typically excite all wavenumbers. Linear growth would then amplify the wavenumber with the largest temporal growth rate. One is led to predict that patterns with k_t are selected, where k_t is such that eigenvalue $\lambda_+(k_t)$ (5.1) is maximal.

On the other hand, one can envision a spatially localized disturbance from the unstable state that is amplified and spreads spatially. One can then compute both spatial spreading speeds and wavenumbers generated at the leading edge of the spatial spread; we outline this construction here and refer to [20, 10] for more details. One considers the linearized equation at

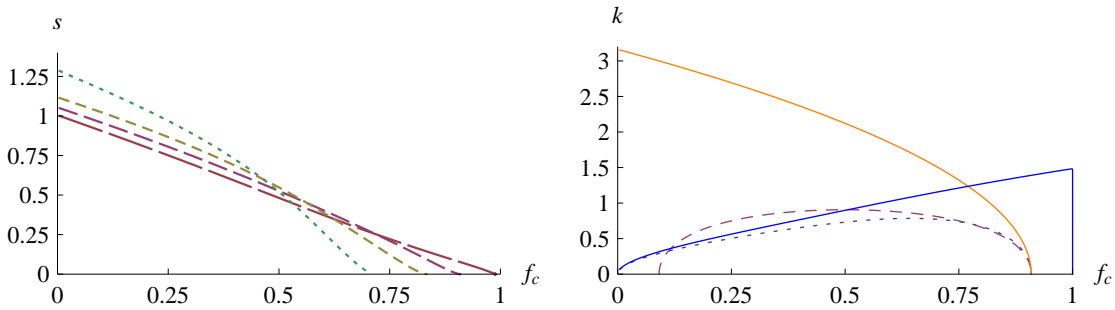


Figure 7.1: On the left, spreading speeds for $d = 0.01, 0.02, 0.05, 0.1, 0.2, 0.4$ as a function of f_c . In both diagrams, $f_e = 1 - f_c$. Spreading speeds are increasing in d for small f_c and decreasing for larger values of f_c . Spreading speeds vanish at $f_e = df_c$ or $f_c = (1 + d)^{-1}$. On the right, a plot of wavenumbers k_s (dotted), k_t (dashed), and k_{lim} (solid) over f_c when $d = 0.1$.

an unstable equilibrium in a frame moving with speed $s > 0$,

$$\begin{aligned} c_t &= c_{\xi\xi} - sc_{\xi} - f_c c - f_e e \\ e_t &= de_{\xi\xi} - se_{\xi} + f_c c + f_e e, \end{aligned} \quad (7.1)$$

and determines whether the instability is convective in nature, that is, if perturbations decay in fixed finite parts of the domain. One defines the linear spreading speed s_{lin} to be the smallest speed where this is the case. Considering s as a parameter, s_{lin} marks the onset of an absolute instability, which is caused by a double root λ of the complex dispersion relation, on the imaginary axis. Here, the complex dispersion relation is obtained from the ansatz $e^{\lambda t + \nu x}$ in the linearized equation (7.1). For $s = 0$, this ansatz gives solutions when

$$d(\lambda, \nu) = \lambda^2 + \lambda(f_c - f_e - (d + 1)\nu^2) + (f_e - df_c)\nu^2 + d\nu^4 = 0.$$

In the comoving frame, the same ansatz gives solutions when $d_s(\lambda, \nu) = d(\lambda - s\nu, \nu)$. Double roots are solutions to $d_s(\lambda, \nu) = 0$ where $\partial_\nu d = 0$, that is, $s\partial_\lambda d = \partial_\nu d$. The imaginary part of the temporal growth rate, $\omega = \text{Im } \lambda$, gives the temporal frequency in a frame moving with speed s , so that the spatial pattern generated by such an oscillation possesses wavenumber $k_s = \omega/s_{\text{lin}}$. One can compute k_s in the Cahn-Hilliard and Allen-Cahn limits and derive expansions. One can also continue solutions from these limits numerically to general values of f_e and f_c . The resulting curves are plotted in Figure 7 for $d = 0.1$, $f_e + f_c = 1$. We also included k_{max} , the maximal unstable wavenumber in a steady frame, in the plot. Curves for other values of f_e, f_c can be obtained by scaling. Curves for other values of d differ only quantitatively; see Figure 7, which contains spreading speeds for several values of d . Roughly, spreading speeds increase with diffusion (as one would expect) in the homogeneous unstable regime and spreading speeds decrease with increasing diffusion in the spinodal regime. Also, temporally and spatially selected wavenumbers, k_t and k_s , are similar for spinodal instabilities but differ significantly for homogeneous instabilities. For instance, one has $k_t = 0$ in the Homogeneous-II-region, $df_e > f_c$, but $k_s > 0$.

We also note that the patterns generated at the leading edge are temporally oscillating in both steady and comoving frames, despite the fact that the system possesses a gradient-structure.

8 Nonlinear spreading: pushed fronts

It is well known that the linear spreading speed computed above may give wrong results when nonlinearities are of “subcritical” type, that is, when they enhance the instability rather than saturating it at low amplitudes. The most prominent example is the Nagumo equation $e_t = de_{xx} + e(1-e)(e-a)$, with unstable equilibrium $e = a, 0 < a < 1/2$. Positive perturbations of $e \equiv a$ spread at the linear spreading speed only when $a > 1/3$. For $a < 1/3$, perturbations spread with the speed $s_{\text{nl}} > s_{\text{lin}}$ of a *pushed front*. The pushed front is a traveling wave that decays faster than fronts at nearby speeds. In the ODE-traveling-wave analysis, it appears as a heteroclinic orbit that connects the unstable manifold of $e = 1$ to the strong stable manifold of $e = a$. We refer to [20, 10, 18] for more details on this transition. Since the Allen-

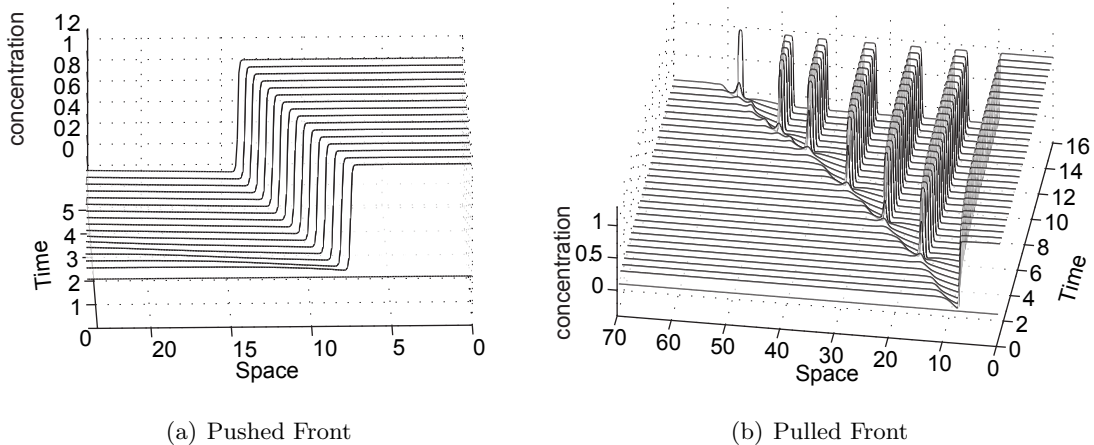


Figure 8.1: *Pushed and pulled fronts $e(t, x)$ in the cubic model.*

Cahn equation appears as a limit when $f_c \rightarrow 0$ in our class of threshold nonlinearities, one suspects that the transition from linear to nonlinear spreading speeds persists. The situation, however, is slightly more complicated. It turns out that pushed fronts do exist, but only for $a < a_*(f_c, d) \ll 1/3$. Pushed fronts destabilize at $a = a_*$ via a Hopf bifurcation, induced by a branch point of the dispersion relation on the imaginary axis. This Hopf bifurcation is *not visible* in the traveling wave equation for positive f_c . To understand this, one can examine the traveling-wave equation (6.2) at $f_c = 0$,

$$\begin{aligned}\theta_\xi &= -s(\theta + (1-d)e - m_\infty) \\ e_\xi &= w \\ w_\xi &= -d^{-1}(sw + e(1-e)(e-a)).\end{aligned}\tag{8.1}$$

One finds the Nagumo-fronts in the (e, w) -equation with the typical transition from pushed to pulled fronts at $a = 1/3$. One can then substitute these fronts into the equation for θ and obtain a unique bounded function θ for any m_∞ . The function θ will however decay with rate $e^{-s\xi}$ at the leading edge, which may be slower than decay rates of the Nagumo front. Since the speed of the pushed front in the Nagumo equation is known explicitly as $s = (a+1)\sqrt{d/2}$, one can calculate explicitly that the steep Nagumo front ceases to be a steep front for (8.1) at $a_*(f_c = 0, d) = d/(2-d)$. In fact, at this value of a_* , a branch point of the dispersion relation that couples θ - and e -equations crosses the origin. A somewhat subtle perturbation analysis shows that this branch point is in fact double and splits into two complex branch point for $f_c > 0$. In other words, the pushed-pulled transition at $a = a_*$ is caused by a Hopf bifurcation in the leading edge; the pushed front continues to exist but is destroyed by oscillations in the leading edge, that eventually accelerate front propagation. We refer to [10] for a more detailed analysis of this situation. Figure 8.1 shows space-time plots of pushed and pulled fronts: pushed fronts are rigidly translating and leave a homogeneous bulk state behind, pulled fronts create a periodic pattern that is unstable and will coarsen after some time. Figure 8.2 shows front speeds computed from direct simulations in comparison to linear spreading speeds and speeds of pushed fronts, both computed using the continuation software AUTO-07P.

9 Existence of coherent pulled fronts

Linear analysis predicts the existence of time-periodic growth in the leading edge of an instability. Direct simulations confirm this oscillatory growth and exhibit coherent (time-periodic) modes of propagation — until coarsening sets in in the wake of the front. A natural question is whether coherent pulled fronts actually exist in a robust fashion, or whether the instability in the wake will destroy coherence. The following proposition shows that such coherent fronts are typical provided that the selected pattern in the wake is stable when considered as a pattern with periodic boundary condition. In that respect, one would expect coherent pulled fronts that create patterns from spinodal states, and coherent pulled fronts that create stable spatially homogeneous states from homogeneous unstable states.

To be precise, we say that a *coherent pulled front* is a front that is time-periodic in a frame moving with the linear spreading speed, with period $T = 2\pi/\omega$, where $\omega = \text{Im } \lambda$ is the

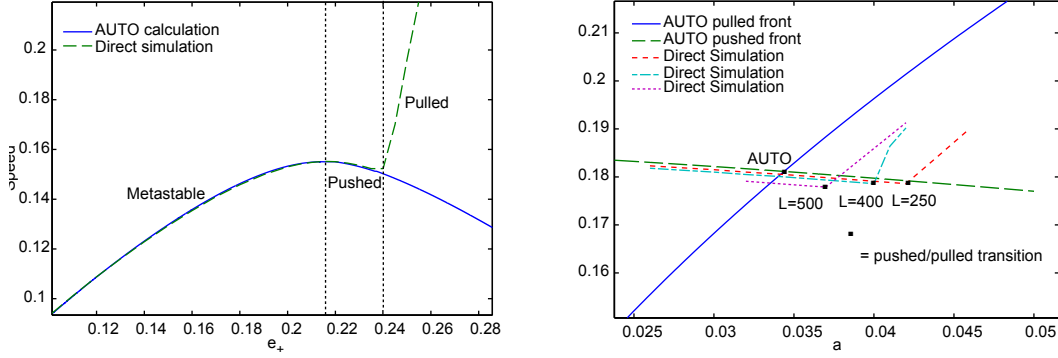


Figure 8.2: On the left, front speeds depending on e_+ , calculated by AUTO (lower parabola) and using direct simulations (top curve). As expected, pulled fronts appear as a smooth continuation of fronts between metastable equilibria. On the right, calculated front speeds for varying a near the pushed-pulled transition using both direct simulation on domains of size L and AUTO. Pulled front speeds converge with increasing domain size, but slowly, in agreement with the predicted slow relaxation $O(1/t)$ of the front speed. Pushed front speeds converge rapidly and agreement with AUTO continuation is limited by discretization step size, only. All calculations use $d = 0.1$.

frequency introduced by the branch point of the dispersion relation: $(c, e)(t, x) = (c, e)(x - s_{\text{lin}}t, \omega t)$, and $(c, e)(\xi, \tau) = (e, c)(\xi, \tau + 2\pi)$. Coherent pulled fronts can be expanded as an infinite Fourier series in the independent periodic variable τ , resulting in an infinite coupled system of traveling-wave equations for the Fourier modes,

$$\begin{aligned} c_\xi^\ell &= v^\ell & e_\xi^\ell &= w^\ell \\ v_\xi^\ell &= -sv^\ell + i\omega\ell c^\ell + \langle e^{-i\ell\tau}, f \rangle & w_\xi^\ell &= d^{-1}(-sw^\ell + i\omega\ell e^\ell - \langle e^{-i\ell\tau}, f \rangle), \end{aligned}$$

where $f = f(\sum_{\ell \in \mathbb{Z}} e^{i\ell\tau} c_\ell + \sum_{\ell \in \mathbb{Z}} e^{i\ell\tau} e_\ell)$, and $\langle u, v \rangle = (2\pi)^{-1} \int_0^{2\pi} \bar{u}(\tau)v(\tau)d\tau$.

Coherent pulled fronts are heteroclinic orbits for this infinite system of ODEs, connecting the homogeneous state at the leading edge to a periodic pattern in the wake; we refer to [16] for details and background on such infinite-dimensional traveling-wave equations. In this infinite system of differential equations, coherent pulled fronts can be obtained as the intersection of stable and unstable manifolds. We say a coherent front is *robust*, if the dimensions of stable and unstable manifolds are complementary, that is, if the intersection can be transverse and the sum of tangent spaces can span the whole space. We refer again to [16, 17] on how to actually count dimensions of the resulting infinite-dimensional manifolds and determine transversality.

Proposition 9.1 *Coherent pulled fronts are robust if the pattern in the wake is stable when considered as a solution to (1.1) with periodic boundary conditions.*

We refer to [10] for a proof of this result. We conjecture that pulled fronts always exist when the system possesses a variational structure; see [18] for a related existence proof. In simulations, we have seen fronts that leave a periodic pattern behind in both spinodal and homogeneous unstable regimes. For spinodal instabilities, the region occupied by the periodic

pattern grows linearly in time. In particular, a coherent front can be observed as a locally uniform state that leaves behind a periodic pattern. From homogeneous unstable equilibria, the front creates a pattern that persists only in a strip of finite width, after which a coarsening process generates a spatially homogeneous pattern. In this case, the coherent front connects spatially homogeneous equilibria as predicted by the above counting arguments.

10 Steady source terms and stationary Liesegang patterns

In our simple class of reaction-diffusion systems (1.1), in the absence of the source term h , steady patterns are quite simple, that is, they are periodic, or they consist of a single layer or spike. One can ask what structure of a reaction-diffusion system would allow for more complicated stationary patterns, in particular patterns on $x \in [0, \infty)$ with Liesegang-type spacing laws. In [19], it is shown that stationary patterns with such geometric spacing laws are typical for a large class of source terms. The results actually hold for more general reaction-diffusion systems with n chemical species $u \in \mathbb{R}^n$,

$$u_t = Du_{xx} + F(u) + h(x), \quad x \geq 0, \quad (10.1)$$

with general, possibly nonlinear boundary conditions $b(u, u_x) = 0$ at $x = 0$ that model inflow and outflow of chemicals. Again, we think of the source term h as the result of an irreversible chemical reaction feeding into our reaction-diffusion system. We suppose that the diffusion matrix $D = \text{diag}(d_j)$ is positive, $d_j > 0$, and the kinetics F are smooth. We assume the source term h is localized near the boundary, $h(x) \sim h_\infty + h_1 e^{-\alpha x}$ as $x \rightarrow \infty$. We set $h_\infty = 0$, possibly absorbing a constant into the kinetics term F . We also assume that the system possesses stationary spikes $u_s(x)$ in the absence of h , which solve $Du_{s,xx} + F(u_s) = 0$ on $x \in \mathbb{R}$. Such spikes are typically exponentially localized, $u_s(x) = u_s(-x) \sim u_\infty + u_1 e^{-\beta|x|}$ for $x \rightarrow \infty$. Again, we may assume $u_\infty = 0$, possibly changing F . We say (10.1) possesses a stationary Liesegang-type pattern $u(t, x) \equiv u_*(x)$ if u_* is close to the superposition of spikes $u_s(x - x_j)$, located at positions x_j with $x_{j+1}/x_j \rightarrow \eta > 1$ as $j \rightarrow \infty$. Under mild assumptions on the linearization at the spike, one can then prove the following.

Proposition 10.1 *Assume that $0 < \alpha < \beta$. Then (10.1) possesses stationary Liesegang patterns with $\eta = \frac{\beta}{\beta - \alpha}$ for appropriate boundary conditions $b(u, u_x)$. Moreover patterns are robust: they depend smoothly on small changes in reaction and diffusion constants or boundary conditions.*

The assumption $\beta > \alpha$ is necessary: stationary Liesegang-type patterns are not robust for $\beta < \alpha$. In other words, slow decay of the source term h compared to the rate of localization of the spike is necessary for Liesegang-type patterns.

A similar result can be formulated when the system possesses layers $u_1(x) \rightarrow u_\pm$, $x \rightarrow \pm\infty$. Stationary Liesegang-type patterns should resemble alternating layers, $u(x) \sim u_1((-1)^j(x - x_j))$, for $x \sim x_j$, $x_{j+1}/x_j \sim \eta$. In other words, they consist of geometrically spaced copies of up- and down-layer solutions.

A simple example is the Allen-Cahn equation $e_t = e_{xx} + e(1 - e^2) + e^{-\alpha x}$, with $0 < \alpha < \sqrt{2}$, which possesses stationary solutions with layers situated at locations with geometrically

increasing distances.

We refer to [19] for precise assumptions and statements, and a somewhat more general setup.

In the specific example of the conversion reaction (1.1), with $h(x) \sim \alpha^2 e^{-\alpha x}$, we can solve for $c + de = h_{-2}(x) \sim \mu + e^{-\alpha x}$, which gives $de_{xx} + f(h_{-2}(x) - de, e) = 0$. When $f(c, e) = e(1 - e)(e - a) + c$, this yields

$$de_{xx} + e(1 - e)(e - a) - de + \mu + e^{-\alpha x} \sim 0.$$

This system satisfies all assumptions of Proposition 10.1 and we can conclude that threshold-type precipitation kinetics F allow for stationary Liesegang-type patterns with geometric spacing law, provided the source term h is stationary and slowly exponentially decaying. Since exponential decay of layers and spikes is rapid, $\beta \sim d^{-1/2}$, for d small, the condition $\alpha < \beta$ is typically satisfied.

11 Moving source terms

Another analytically tractable example of source terms is the case of a moving source $h(t, x) = h(x - st)$ for some speed $s > 0$. We think of this moving source as stemming from a reaction front in a second equation. Although reaction fronts in experiments leading to the formation of Liesegang patterns typically exhibit diffusive spread, $s = s(t) \sim 1/\sqrt{t}$, we found that the analysis gives valuable insight into those experiments, too. We are interested in transitions to unstable states triggered by such a moving source. More precisely, we look for a traveling wave to the reaction-diffusion system that connects a stable state ahead of the front $\xi = x - st = +\infty$ to an unstable state in the wake $\xi = -\infty$. The traveling-wave equation becomes

$$\begin{aligned} \theta_\xi &= -s(\theta + (1 - d)e - m_\infty) - H(\xi) \\ e_\xi &= w \\ w_\xi &= -d^{-1}(sw + e(1 - e)(e - a)). \end{aligned} \tag{11.1}$$

Here, $H(\xi) = -\frac{1}{s} \int_\xi^\infty h(\zeta) d\zeta$, and $m_\infty = e(\infty) + c(\infty)$. Note that traveling waves now respect the total mass change, $\delta m = \int_{\mathbb{R}} h(x - st) dt$.

$$e(-\infty) + c(-\infty) = e(+\infty) + c(+\infty) + \delta m.$$

One can analyze the existence of traveling waves in various limits, when $h(\xi) \sim \delta(\xi)$ is sharply localized, and when $d \ll 1$. Instead, we emphasize here a crude *counting argument*. We analyze the linearized properties of equilibria (c_\pm, e_\pm) in (11.1) and infer information on which type of traveling waves is likely to occur. This counting argument is quite robust and holds for much more general systems. It also lies at the heart of the proof of Proposition 9.1 on the robustness of pulled modulated fronts.

Proposition 11.1 *Fronts that connect a stable state ahead to a spinodal unstable state in the wake are robust. Fronts that connect a stable state ahead to a homogeneous unstable state are not robust: there exist arbitrarily small perturbations of the forcing function, that preserve the total mass change δm but destroy the traveling wave.*

One therefore expects that homogeneous unstable states are not left behind a moving source in a typical setup. One does however expect to see plateaus with spinodal unstable states in the wake of moving sources. On those plateaus, small disturbances would then initiate a pattern-forming pulled front. The proof of the proposition is based on the computation of dimensions of stable and unstable manifolds near equilibria (c_{\pm}, e_{\pm}) . One finds from a direct computation that stable states possess a two-dimensional stable manifold and a one-dimensional unstable manifold in the traveling-wave system (11.1). Spinodal states have the same stable and unstable dimension, while homogeneous unstable states are stable. Intersections between the two-dimensional stable manifold of a stable state and the one-dimensional unstable manifold of a spinodal unstable state are typically transverse and robust. Intersections between the two-dimensional stable manifold of the stable state and the 0-dimensional unstable manifold (consisting of the equilibrium state itself) of a homogeneous unstable state are not robust. We refer to [10] for a more general argument that applies to general reaction-diffusion systems without relying on explicit computations.

12 Liesegang patterns – the role of the conversion rate

We show a number of simulations that illustrate the role of the conversion rate f on the formation of Liesegang patterns. In the following, we consider (1.1) with a source term $h(t, x) = a(t, x)b(t, x)$, where

$$a_t = a_{xx} - ab, \quad b_t = d_b b_{xx} - ab,$$

and $a(0) = a_0 > 0$, $a_x(0) = b_x(0) = b_x(L) = 0$, and $a(0, x) \equiv 0$, $b(0, x) \equiv b_0 > 0$.

Spikes versus layers We illustrate the differences between the smoothed versions g_1 and g_2 of supersaturation kinetics, (4.2). The main difference is caused by the absence of layers at small diffusion rates with g_1 -kinetics. As a consequence, the moving ab -front generates spikes with increasing amplitude for g_1 and layers of increasing width for g_2 .

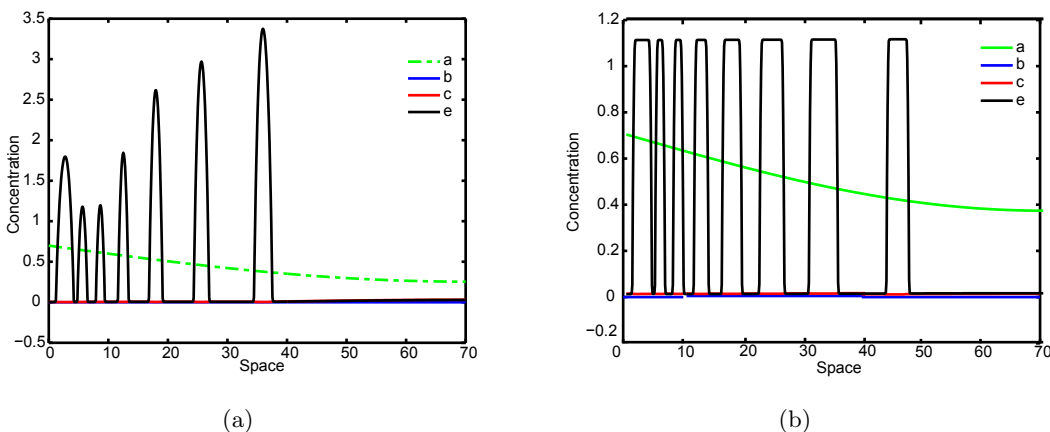


Figure 12.1: 1(a): Simulation using kinetics g_1 from (4.2). 1(b): Simulation using kinetics g_2 from (4.2).

Spinodal versus bistable We generally found that Liesegang patterns were less likely to develop for bistable f , that is, the ranges of admissible parameters a_0, b_0 , and d_b were much smaller. The following two series of snapshots illustrate the formation of Liesegang patterns with spinodal versus bistable cubic conversion rate. In the spinodal regime, Figure 2(a), the concentrations of c and e increase up to a plateau from where the instability develops, as predicted by the analysis in Section 11. In the bistable regime, Figure 12.3, the spikes form immediately once the source term has caused an increase of the c -concentration above the threshold. We have seen but not yet corroborated differences in scaling laws that should be attributed to these different mechanisms.

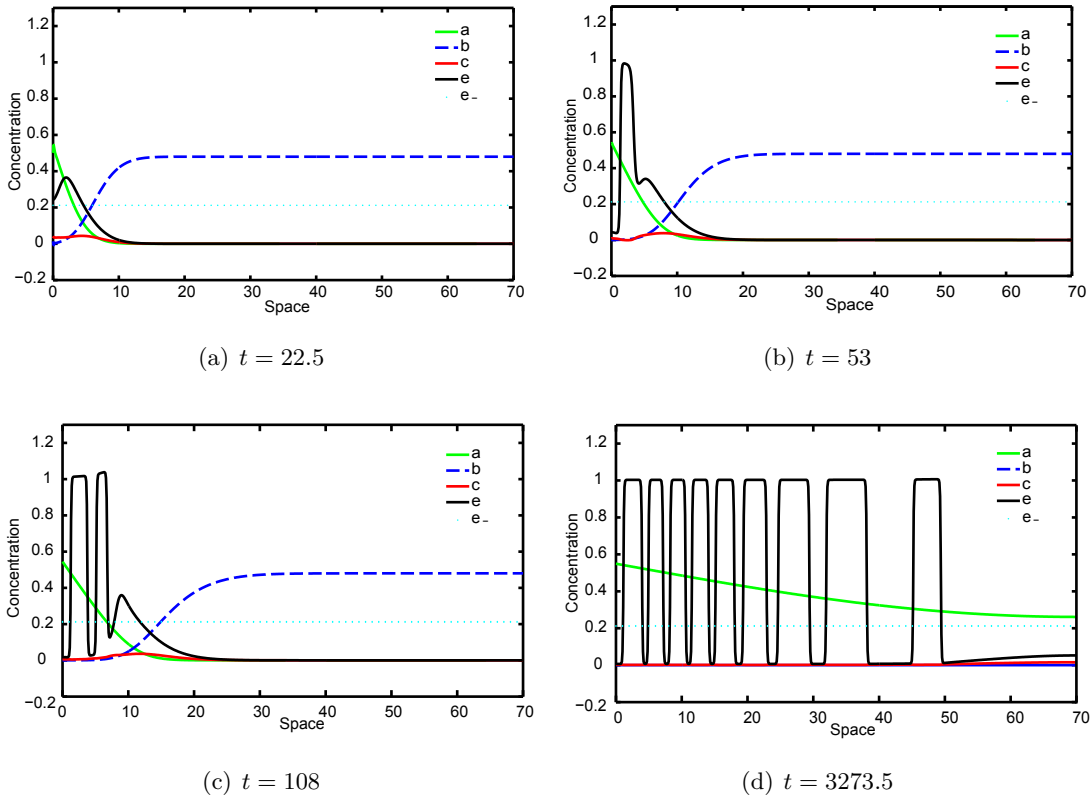


Figure 12.2: Formation of Liesegang pattern with cubic kinetics in the spinodal regime, $\kappa = 0.7$.

Revert patterns The simulations in the spinodal regime suggest that the wavenumber behind the moving source is related to wavenumber selection from a spinodal instability as discussed in Section 7. Since the moving source is decaying in amplitude, the spinodal decomposition develops from equilibria (c, e) with decreasing amplitude. For e close to e_- , this implies that the strength of the instability, measured by f_e , decreases, and therefore k decreases; see Figure 7. The behavior of f_e as c, e decrease along the nullcline $f(c, e) = 0$ does however depend on the precise shape of the kinetics f .

In particular, one can easily construct examples where f_e is increasing for a wide range of

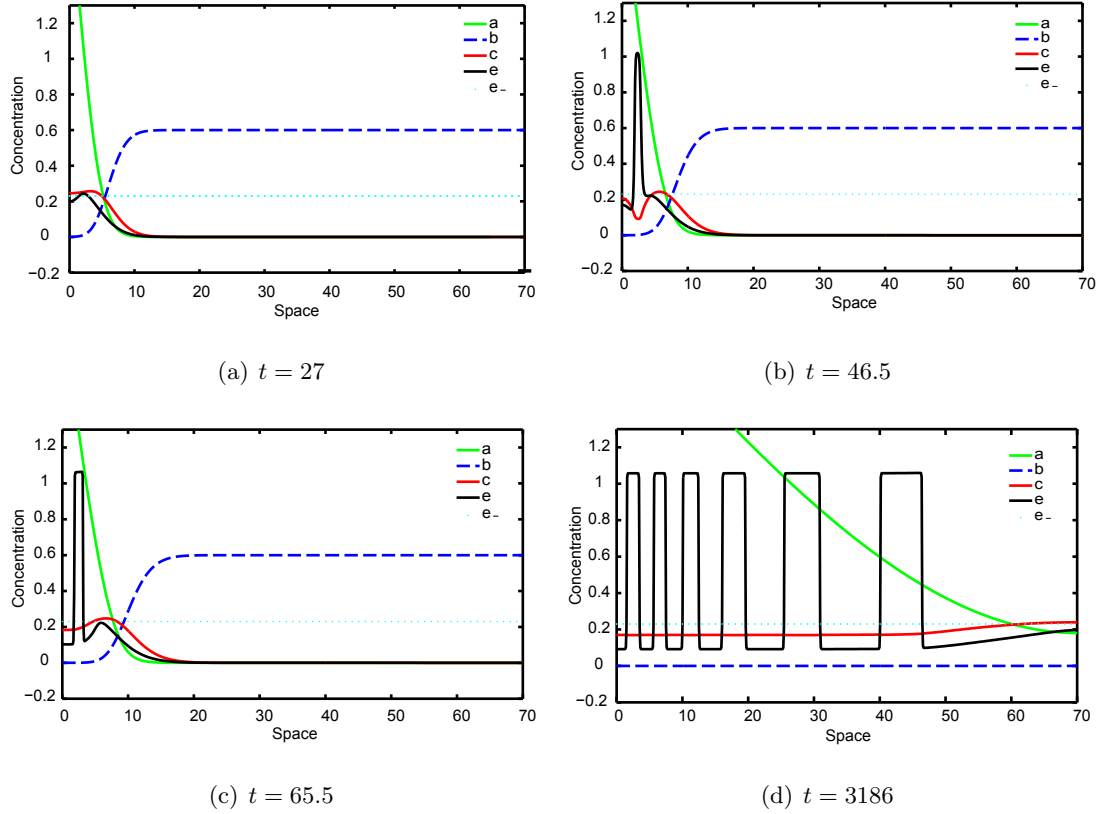


Figure 12.3: Formation of Liesegang pattern with cubic kinetics in the bistable regime, $\kappa = 5$.

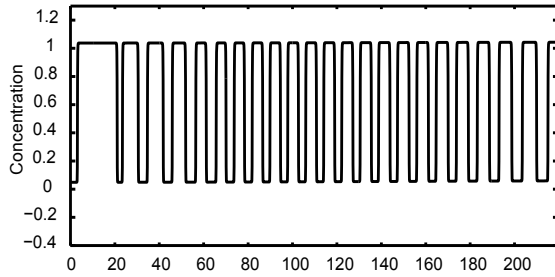


Figure 12.4: Revert Pattern: $\alpha = 0.2, \beta = 2, \kappa = 1.5, a_0 = 3, b_0 = 0.55, L = 300, d_e = 0.0001, d_b = 0.85$. Note how around $L = 120$ the pattern switches back into regular Liesegang patterns.

equilibrium concentration $\bar{f}(c, e)$. An explicit example is

$$\bar{f}(c, e) = \alpha e^{-\beta} f(c, e) = \alpha e^{-\beta e} [c + \kappa e(1 - e)(e - \alpha)] \quad (12.1)$$

where α and β are positive constants. Figure 12.4 illustrates the effect on Liesegang patterns: the pattern is reversed over a wide range, spacing between layers is decreasing.

13 Summary and conclusions

We presented an overview of coherent structures in threshold reaction-diffusion models for precipitation. The main distinction between different models appears to be the presence of bistability in some models versus the mere existence of spinodal instabilities in other models. Generally speaking, spinodal instabilities appear to facilitate the appearance of patterns, while bistable characteristics favor bulk states in the wake of fronts. In agreement with these general

characteristics, we found it much easier to numerically generate Liesegang patterns in systems with spinodal instability, only. The simplest distinguishing feature between the two models is the presence of multiple homogeneous steady-states: only systems with bistable characteristics will exhibit multiple steady-states for fixed concentration in a sufficiently small domain. As a novel phenomenon, we exhibit a transition from pushed to pulled front propagation in our models in the bistable regime. Phenomenologically, this transition discriminates between pattern-forming spread of an instability versus immediate formation of a bulk state in the wake of an instability. We hope that the general phenomenological description of dynamics presented here can help discriminate between models in experimental contexts.

References

- [1] T. Antal, I. Bena, M. Droz, K. Martens, and Z. Rácz. *Guiding fields for phase separation: Controlling Liesegang patterns*. Phys. Rev. E **76** (2007), 046203.
- [2] T. Antal, M. Droz, J. Magnin, Z. Racz. *Formation of Liesegang Patterns: A Spinodal Decomposition Scenario*. Phys. Rev. Lett. **82** (1999), 2880-2883.
- [3] P. Bates, P. Fife, R. Gardner, C. Jones. *The existence of travelling wave solutions of a generalized phase-field model*. SIAM J. Math. Anal. **28** (1997), 60–93.
- [4] G. Caginalp and Y. Nishiura. *The existence of travelling waves for phase field equations and convergence to sharp interface models in the singular limit*. Quart. Appl. Math. **49** (1991), 147–162.
- [5] G. Caginalp. *An analysis of a phase field model of a free boundary*. Arch. Ration. Mech. Anal. **92** (1986), 205–245.
- [6] M. Droz. *Recent Theoretical Developments on the Formation of Liesegang Patterns*. J. Stat. Physics **101** (2000), 509–519.
- [7] C. Dupaix, D. Hilhorst, I.N. Kostin. *The viscous Cahn-Hilliard Equation as a Limit of the Phase Field Model: Lower Semicontinuity of the Attractor*. J. of Dyn. Diff. Eq. **11** (1999), 333.
- [8] K. Glasner. *Traveling waves in rapid solidification*. Electron. J. Differential Equations **16** (2000).
- [9] K. Glasner. *Rapid growth and critical behaviour in phase field models of solidification*. European J. Appl. Math. **12** (2001), 39–56.
- [10] R. Goh, S. Mesuro, A. Scheel. *Coherent structures in threshold models for precipitation*. In preparation.
- [11] D. Hilhorst, R. van der Hout, M. Mimura, and I. Ohnishi. *Fast reaction limits and Liesegang bands*. Free boundary problems, 241–250, Internat. Ser. Numer. Math., 154, Birkhuser, Basel, 2007.
- [12] D. Hilhorst, R. van der Hout, M. Mimura, and I. Ohnishi. *A Mathematical Study of the One-Dimensional Keller and Rubinow Model for Liesegang Bands*. J. Stat. Phys. **135** (2009), 107–132.
- [13] J.B. Keller and S. Rubinow. *Recurrent precipitation and Liesegang rings*. J. Chem. Phys. **74** (1981), 5000–5007.

- [14] A. Pogan and A. Scheel. *Instability of Spikes in the Presence of Conservation Laws*. To appear in *Z. Angew. Math. Phys.*
- [15] A. Pogan and A. Scheel. *Stability and instability of patterns in the presence of conservation laws*. In preparation.
- [16] B. Sandstede and A. Scheel. *Defects in oscillatory media: toward a classification*. *SIAM J. Appl. Dyn. Syst.* **3** (2004), 1–68.
- [17] B. Sandstede and A. Scheel. *Relative Morse indices, Fredholm indices, and group velocities*. *Discrete Contin. Dyn. Syst.* **20** (2008), 139–158.
- [18] A. Scheel. *Coarsening fronts*. *Arch. Ration. Mech. Anal.* **181** (2006), 505–534.
- [19] A. Scheel. *Robustness of Liesegang patterns*. *Nonlinearity* **22** (2009), 457–483.
- [20] W. van Saarloos. *Front propagation into unstable states*. *Phys. Rep.* **386** (2003), 29–222.